Available online at www.sciencedirect.com

SciVerse ScienceDirect

Ceramics International 39 (2013) 3151–3155

CERAMICS INTERNATIONAL

www.elsevier.com/locate/ceramint

Synthesis and characterization of Pr_6O_{11} nanopowders

Branko Matović*, Jelena Pantić, Marija Prekajski, Nadežda Stanković, Dušan Bučevac, Tamara Minović, Maria Čebela

Materials Science Laboratory, Vinča Institute of Nuclear Sciences, University of Belgrade, PO Box 522, 11001 Belgrade, Serbia

Received 6 August 2012; received in revised form 28 September 2012; accepted 28 September 2012
Available online 5 October 2012

Abstract

Amorphous Pr_6O_{11} powder was obtained by applying self-propagating room temperature method (SPRT). After calcination, the amorphous powder converted to nanometric Pr_6O_{11} powder with cubic fluorite-type structure. Powder properties such as crystallite size, lattice strain and lattice parameter were studied by X-ray diffraction (XRD) at room temperature. The crystallite size was estimated by means of the full width at half maxima (FWHM) of XRD peaks. Williamson–Hall plots were used to determine the lattice strain whereas the Ritveld analysis was employed for crystal structure refinement. It was found that the powder properties are affected by both calcination temperature and duration of thermal treatment. The crystallite size varied from 5 to ~250 nm, whereas the lattice parameter varied from 5.461 to 5.494 Å. The powder obtained after four-hour long calcination was almost free of internal strain.

Keywords: A. Calcination; B. X-ray methods; Pr-oxides

1. Introduction

Praseodymium oxide (Pr_6O_{11}) has become a promising material for functional application. It has already been used in production of high-temperature pigments, catalysts, promoters and stabilizers in combustion catalysis, oxygen-storage components, and ceramics with high electrical conductivity [1–5]. Currently, there are very limited number of techniques that can be effectively used for preparation of micro- and nanosized praseodymium oxide. Pr_6O_{11} is traditionally synthesized by solid-state reactions such as high-temperature thermolysis of praseodymium salts, calcination of as-prepared Pr-hydroxide [6,7], molten salt method [8], facile template-free precipitation route [9], electrospinning of an aqueous sol–gel consisting of Pr-nitrate and polyvinyl acetate [10].

In this paper, a simple route for synthesis of pure, crystalline, Pr_6O_{11} compound is presented. The simplicity of the manufacturing route makes it a promising method for the scaling-up of Pr_6O_{11} nanopowder production.

2. Material and methods

The Pr_6O_{11} powder was prepared by a SPRT method using Pr-nitrate (Aldrich, USA) and NaOH (p.a. Zorka, Serbia) as starting materials. The composition of reacting mixture was calculated according to the nominal composition of the final product of the following equation:

$$6Pr(NO_3)_3 \cdot 6H_2O + 18\ NaOH + O_2 \rightarrow Pr_6O_{11} + 18\ NaNO_3 + 45\ H_2O \quad (1)$$

This reaction can be initiated by short (few minutes) hand mixing of the mixture of reactants in a mortar. The products were centrifuged in order to eliminate $NaNO_3$. After draying at 60 °C in air, the obtained powder was calcined at temperature ranging from 400 to 800 °C. The thermal treatment was 1–4 h long.

The crystalline phases of the obtained powders were identified by means of X-ray diffraction (XRD) using Siemens D-5000 XRD diffractometer with CuKα radiation at room temperature. The measurements were performed in the 2θ range from 10 to 80° in a continuous scan mode with a step width of 0.02° and at a scan rate of 1° 2θ/min. Before the measurement, the angular correction was done by high quality Si standard. Data for structural refinement

*Corresponding author. Tel.: +381113408 753; fax: +381113408224.
E-mail address: mato@vinca.rs (B. Matović).

0272-8842/$ - see front matter © 2012 Elsevier Ltd and Techna Group S.r.l. All rights reserved.
http://dx.doi.org/10.1016/j.ceramint.2012.09.098

of sample calcined at 600 °C were taken in the 2θ range 20–120°, with the step of 0.02° and prolonged scanning time of 12 s per step. The refinement was performed with the FullProf computer program [11–13] which adopts the Rietveld calculation method. The TCH pseudo-Voigt profile function was used [14]. To take instrumental broadening into account, the XRD pattern of a standard specimen CeO_2 was fitted by the convolution of the experimental TCH pseudo-Voigt function. Morphology and texture of the obtained powders were studied by means of Scanning electron microscopy (SEM) using a JEOL 6300F microscope at 3 kV accelerating voltage.

3. Results and discussion

According to X-ray diffraction analysis, the powder obtained at room temperature (as-prepared) is amorphous. It was also found that the subsequent calcination promotes crystallization of Pr_6O_{11}. Typical XRD patterns of Pr_6O_{11} powders calcined at different temperatures for 1 h are shown in Fig. 1. As can be seen, the pattern of sample calcined at 400 °C exhibits very diffuse diffraction lines, in such way that the identification of atomic planes is impossible. However, XRD patterns of samples calcined at higher temperatures show single Pr_6O_{11} phase. All peaks of Pr_6O_{11} samples can be indexed to a cubic fluorite crystal structure (Fm3m – 225 S.G.) with the lattice constant of a_o=0.546(7) nm (JCPDS 42–1121). Peaks related to the isolated Pr-hydroxides, impurities or the other Pr-oxide phases are not observed. Furthermore, Fig. 1 reveals that the peaks in XRD patterns of samples calcined at 500 and 600 °C are considerably broadened indicating small crystallite size or/and strain. As expected, the further increase in calcination temperature causes sharpening of the diffraction lines, which is the result of increased crystallite size. It appears that temperature of 800 °C is sufficiently high to obtain well crystallized powder after one-hour long calcination. The inserted diagram indicates that prolonged, four-hour long, calcination can cause crystallization even at temperature as low as 400 °C.

Having concluded that both calcination time (dwell time) and temperature have strong effect on crystallization it would be of significant importance to study the effect of these parameters on crystallite size. The as-prepared powder was calcined in temperature range from 500 to 800 °C for different times. The values for crystallite size which were calculated from XRD data using Scherrer's method [15] are presented in Fig. 2. As expected, the crystallite size increases with calcination temperature for all dwell times. It is important to stress that the increase in crystallite size is the most exaggerated when temperature is raised from 700 to 800 °C. Namely, the average crystallite size of samples calcined for 4 h increased moderately from less than 15 nm at 500 °C to 45 nm at 700 °C. However, further increase in calcinations temperature to 800 °C causes a considerable increase in crystallite size to above 250 nm. It can be concluded that one has to keep calcination temperature below 800 °C in order to obtain fine powders. Fig. 2 also shows the effect of dwell time on the crystallite size of samples calcined at different temperatures. It is interesting to note that the effect of dwell time is quite modest when it comes to the samples calcined at temperatures lower than 800 °C. An increase in dwell time from 1 to 4 h at 700 °C causes an increase in crystallite size from 30 to 45 nm. This increase is quite small when compared to the increase in crystallite size after calcination at 800 °C. As Fig. 2 indicates, an increase in dwell time from 1 to 4 h at 800 °C causes an increase in crystallite grain size from 100 nm to more than 250 nm. Besides the crystallite size, strain is another important parameter in powder characterization.

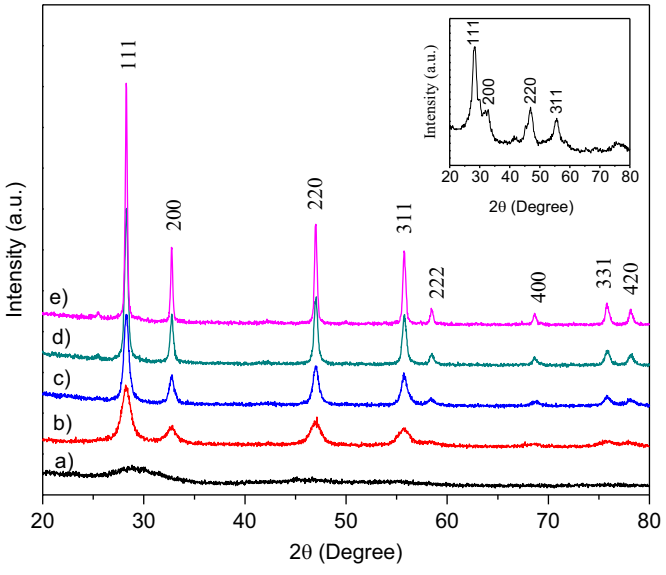

Fig. 1. X-ray diffraction patterns of Pr_6O_{11} powders annealed at 400 °C (a), 500 °C (b), 600 °C (c), 700 °C (d) and 800 °C (e) for 1 h. Insert: XRD pattern of Pr_6O_{11} powders annealed at 400 °C for 4 h.

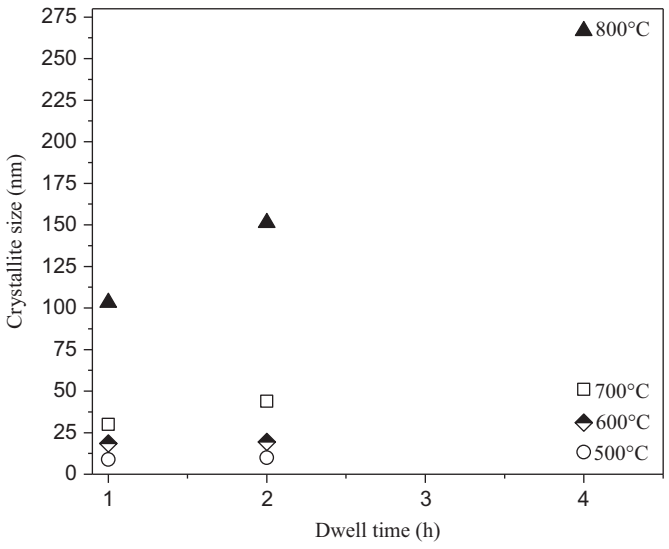

Fig. 2. Crystallite size as a function of temperature and dwell time.

The internal strain of samples calcined at different temperature for 4 h was estimated from the Williamson–Hall plots (Fig.3) which were drawn using following equation [16]:

$$\boldsymbol{\beta}_{\text{total}} \cdot \cos\boldsymbol{\theta} = 0.9\,\boldsymbol{\lambda}/\,\mathrm{D} + 4\,\Delta d/\,d \cdot \sin\boldsymbol{\theta} \quad (2)$$

where β_{total} is the full width half maximum of the XRD peak, λ is the incident X-ray wave length, θ is the diffraction angle, D is the crystallite size and Δd is the difference of the d spacing corresponding to a typical peak. The obtained values of lattice strain along with the values of crystallite size and lattice parameter are listed in Table 1. It is evident from Eq. (2) that the strain of nanocrystals, $\Delta d/d$, can be determined from the slope of function $\beta \cdot \cos\theta$ vs. $\sin\theta$ whereas crystallite size, D, can be determined from the y-intercept. As Fig. 3 shows, the slope, and therefore strain, decreases with an increase in calcination temperature. This decrease in internal strain is considered to be the consequence of an intensive ordering of atoms during calcinations at high temperature which decreases the dislocation concentration in crystal lattice. It is important to stress that the slope for powders calcined at high temperature such as 800 °C for 4 h is close to zero which indicates that material is free of internal strain, i.e., fully crystalline. Furthermore, it is well known that the significant amount of strain is localized at the surface of crystallites as result of a high concentration of broken

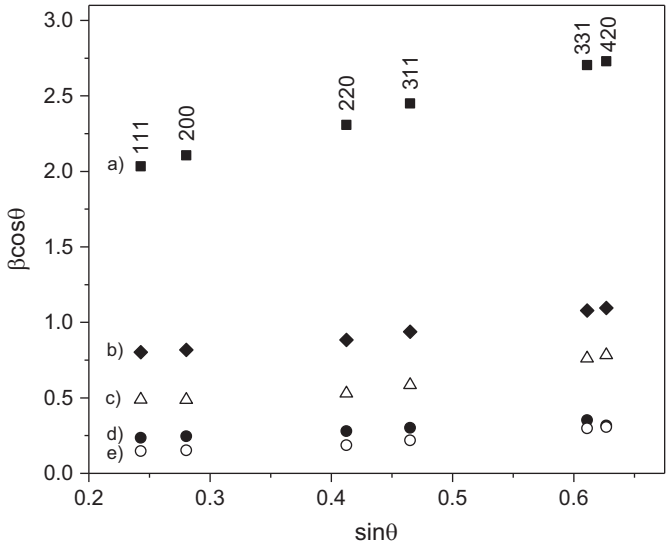

Fig. 3. Williamson–Hall plot of the Pr_6O_{11} powders after four-hour long calcination at 400 °C (a), 500 °C (b), 600 °C (c) and 700 °C (d) and 800 °C (e).

Table 1
Unit cell parameters, crystallite size and lattice strain of Pr_6O_{11}.

Temperature (°C)	400	500	600	700	800
Lattice parameter (Å)	5.494(9)	5.461(4)	5.462(4)	5.462(7)	5.465(5)
Crystallite size (nm)	5.00	13.3	21.7	45.2	> 250
Lattice strain (ε)	7.94×10^{-3}	3.37×10^{-3}	2.02×10^{-3}	1.11×10^{-3}	–

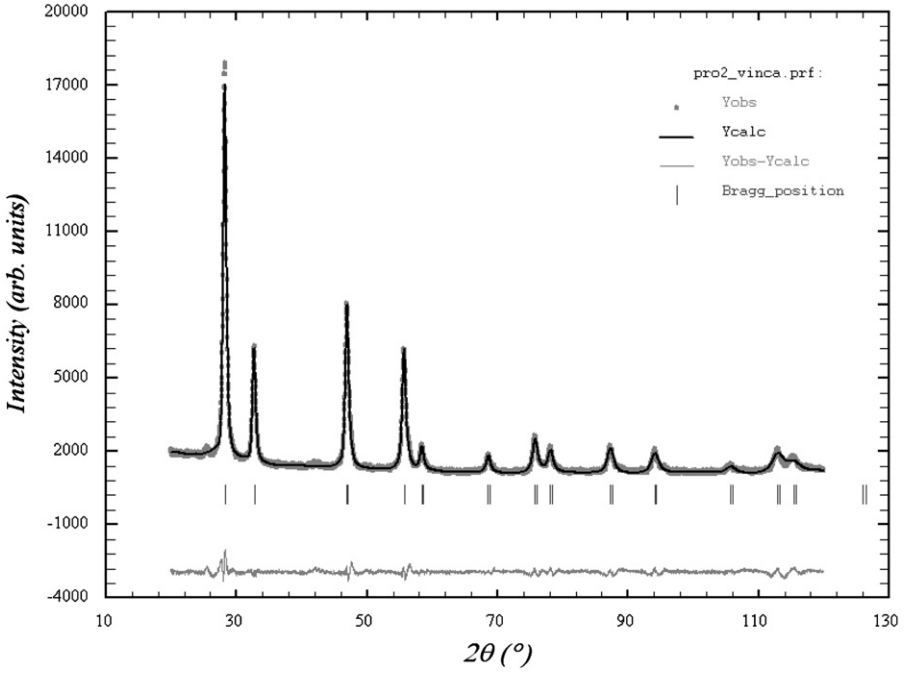

Fig. 4. XRD pattern of sample calcinated at 600 °C for 4 h after structural refinement procedure using the Rietveld's method. A difference (observed − calculated) plot is shown beneath. Tick marks above the difference data indicate the reflection position.

bonds. Therefore it is expected that the internal strain decreases with an increase in the crystallite size due to reduction in the specific surface of crystallites. As mentioned before, the crystallite size of powder calcined at 800 °C for 4 h was more than 250 nm which resulted in a very small lattice strain (Table 1).

The values of unit cell parameter a_o (Å) for samples calcined at different temperatures for 4 h are presented in Table 1. It is interesting to note that the cell parameter of Pr_6O_{11} obtained at the lowest temperature, i.e., 400 °C is considerably higher than that of samples obtained at higher temperatures. Although one can find unexpected that the lattice parameter decreases with increasing crystallite size (temperature), this phenomenon was found in various nanocrystalline materials [17,18]. In the case of Pr_6O_{11}, this behavior can be ascribed to the presence of Pr^{3+} cations [19] in samples calcined at low temperature. Pr_6O_{11} is a nonstoichiometric compound in which praseodymium is in the form of either Pr^{3+} or Pr^{4+} cation. There are two effects of the presence of Pr^{3+} on lattice expansion. The first one is based on the fact that the ionic radius of Pr^{3+} (0.1126 nm) is larger than that of Pr^{4+} which is determined to be 0.096 nm. The presence of larger anion increases the length of Pr – O bond which in turn causes the increase in overall lattice parameter. The second effect is related to the presence of oxygen vacancies which were introduced in the lattice as charge compensation effect of substitution of Pr^{4+} with Pr^{3+} ions. The presence of oxygen vacancies causes an extension of certain bonds due to unbalanced atomic forces. Thus, the large lattice parameter of sample calcined at 400 °C is due to the large concentration of Pr^{3+} cations and therefore large concentration of oxygen vacancies at low calcination temperature. However, an increase in temperature to 500 °C results in the valence change of praseodymium from Pr^{3+} to Pr^{4+} due to higher thermodynamic stability of Pr^{4+} at higher temperature in ambient atmosphere. The result of this transformation is a decrease in lattice parameter of sample calcined at 500 °C. The equilibrium concentrations of Pr^{3+} and Pr^{4+} are achieved at approximately 500 °C. Very small increase in the lattice parameter with further increase in calcinations temperature (Table 1) is within the standard errors.

Rietveld refinement was carried out on sample calcined at 400 °C for 4 h using data reported by Schreiner (JCPDS 42–1121) [20] as the starting structural model. The X-ray powder pattern after the refinement is shown in Fig. 4. It reveals that all reflection can be indexed to a pure face-centered cubic phase of the Pr_6O_{11} crystal with refined lattice constant $a=5.46963(4)$ Å. This constant is slightly larger than the literature value ($a=5.4678$ Å) which is quite expected when it comes to nanostructure materials. The refined structure and microstructure parameters show that the crystallite size is in nanometric range of about 17 nm. The reasonable values of R factors ($Rp=14.3$, $Rwp=12.4$, $R_B=2.07$ and $Ch^2=3.28$) confirm a good refinement.

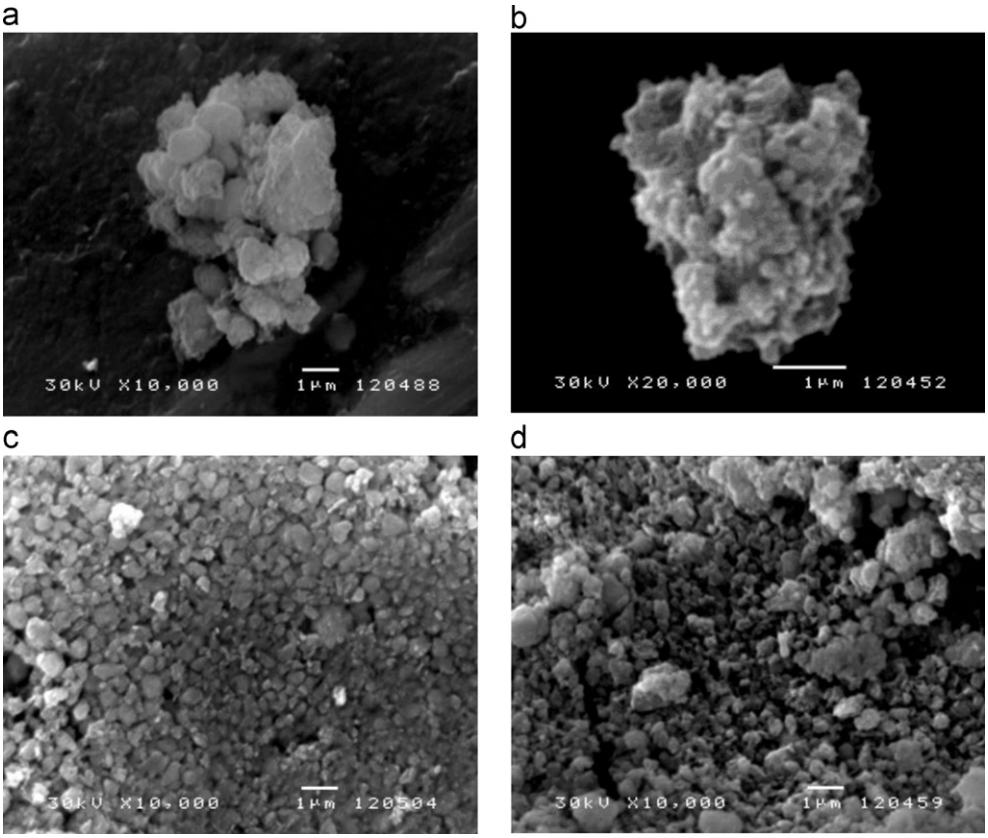

Fig. 5. SEM images of nano Pr_6O_{11} annealed at different temperatures for 1 h: 400 °C (a); 500 °C (b); 600 °C (c) and 700 °C (d).

The morphologies of powders obtained after four-hour long calcination at different temperatures are presented in Fig. 5. As Fig. 5a reveals, the powder obtained at low temperature such as 400 °C is in the form of big clusters of agglomerates. The average diameter of agglomerates is approximately 4 μm whereas the diameter of clusters is close to 10 μm. It is believed that the pronounced agglomeration is the result of very small particle size. This reasoning is supported by the fact that further increase in calcination temperature and consequent increase in particle size leads to a reduction in the agglomerate size. As Fig. 5b shows, the diameter of agglomerates in sample calcined at 500 °C is below 2 μm. The reduction in agglomerate size is even more pronounced in the samples calcined at 600 °C. As Fig. 5c indicates, all agglomerates are below 1 μm in diameter which is considered to be a result of low affinity to agglomeration of coarse powder obtained at higher temperature. It can be also noted that the agglomerates in sample calcinated at 600 °C are more compact which can be ascribed to the inevitable crystallite growth. Finally, the increase in calcinations temperature to 700 °C leads to bimodal distribution of agglomerate size. Fig. 5d shows that the diameter of majority of agglomerates is less than 0.5 μm whereas the certain number of agglomerates can be up to 2 μm in diameter. Having concluded that the crystallite size in sample calcined at 700 °C for 4 h was ~45 nm it can be estimated that the big agglomerates consist of approximately 50 crystallites which grow together at high temperature.

4. Conclusions

Self-propagating room temperature method (SPRT) is a simple route which allows to fabricate amorphous praseodymium oxide from Pr-nitrate and sodium hydroxide. Thermal treatment at temperature above 400 °C leads to a conversion of amorphous oxide into crystalline Pr_6O_{11}. High amount of microstrain was found in the crystalline Pr_6O_{11} obtained at lower calcination temperatures. The internal microstrain decreases with increasing calcination temperature. Large crystallites (> 250 nm) obtained at 800 °C are free of microstrain. Ritveld refinement confirmed a single Pr_6O_{11} phase.

Acknowledgment

This project was financially supported by the Ministry of Education and Science of Serbia (project number: 45012).

References

[1] P. Ŝulcovă, J. Therm, Thermal synthesis of the CeO_2–PrO_2–Nd_2O_3 pigments, Analysis and Calorimetry 82 (2005) 51.
[2] K. Asami, K. Kusakabe, N. Ashi, Y. Ohtsuka, Synthesis of ethane and ethylene from methane and carbon dioxide over praseodymium oxide catalysts, Applied Catalysis A: General 156 (1997) 43.
[3] S. Bernal, F.J. Botana, G. Cifredo, J.J. Calvino, A. Jobacho, J.M. Rodriguez- Izquierdo, Preparation and characterization of a praseodymium oxide to be used as a catalytic support, Journal of Alloys and Compounds 180 (1992) 271–279.
[4] M. Kawabe, H. Ono, T. Sano, M. Tsuji, Y. Tamaura, Thermochemical oxygen pump with praseodymium oxides using a temperature-swing at 403–873 K, Energy 22 (1997) 1041–1049.
[5] S. Shrestha, C.M.Y. Yeung, C. Nunnerley, S.C. Tsang, Comparison of morphology and electrical conductivity of various thin films containing nano-crystalline praseodymium oxide particles, Sensors and Actuators A 136 (2007) 191–198.
[6] P.X. Huang, F. Wu, B.L. Zhu, G.R. Li, Y.L. Wang, X.P. Gao, H.Y. Zhu, T.Y. Yan, W.P. Huang, M. Zhang, D.Y. Song, Praseodymiumhydroxide and oxide nanorods and Au/Pr_6O_{11} nanorod catalysts for CO oxidation, Journal of Physical Chemistry B 110 (2006) 1614–1620.
[7] L. Ma, W. Chen, J. Zhao, Y. Zheng, X. Li, Z. Xu, Microwave-assisted synthesis of praseodymium hydroxide nanorods and thermal conversion to oxide nanorod, Materials Letters 61 (2007) 1711–1714.
[8] X. Wang, J. Zhuang, Y.D.Li Eur, Pr6O11 single-crystal nanotubes from a molten-salt synthetic method, Journal of Inorganic Chemistry (2004) 946–948.
[9] L. Yan, R. Yu, G. Liu, X. Xing, A facile template-free synthesis of large-scale single crystalline $Pr(OH)_3$ and Pr_6O_{11} nanorods, Scripta Materialia 58 (2008) 707–710.
[10] M.S. Hassan, Y.S. Kang, B.S. Kim, I.S. Kim, H.Y. Kim, M.S. Khill, Synthesis of praseodymium oxide nanofiber by electrospinning, Superlattices and Microstructures 50 (2011) 139–144.
[11] J. Rodriguez-Carvajal, FullProf computer program, 1998, 〈ftp://charybde.saclay.cea.fr/pub/divers/fullprof.98/windows/winfp98.zip〉.
[12] J. Rodriguez-Carvajal, Recent advances in magnetic structure determination by neutron powder diffraction, Physica B 192 (1993) 55–69.
[13] J. Rodríguez-Carvajal, Recent Developments of the Program FULLPROF, in Commission on Powder Diffraction (IUCr). Newsletter 26 (2001) 12–19.
[14] D. Balzar, N. Audebrand, M.R. Daymond, A. Fitch, A. Hewat, J.I. Langford, A. Le Bail, D. Louer, O. Masson, C.N. McCowan, N.C. Popa, P.W. Stephens, B.H. Toby, Size–strain line-broadening analysis of the ceria round-robin sample, Journal of Applied Crystallography 37 (2004) 911–924.
[15] B.D. Cullity, S.R. Stock, Elements of X-ray Diffraction-third, Ed., Prentice Hall, New Jersey, 2001.
[16] C. Suryanarayana, M. Grant Norton, X-ray Diffraction: A Practical Approach, Springer, New York, 1998.
[17] S.H. Tolbert, A.P. Alvisiatos, High pressure phase transitions in semiconductor nanocrystals, Annual Review of Physical Chemistry 46 (1995) 595–625.
[18] K. Lu, Y.H. Zhao, Experimental evidences of lattice distortion in nanocrystalline materials, Nanostructured Materials 12 (1999) 559–562.
[19] L. Yan, X.R. Xing, R.B. Yu, J.X. Davis, J. Chen, G.R. Liu, Facile alcohothermal synthesis of large-scale ceria nanowires with organic surfactant assistance, Physica B 390 (2007) 59–64.
[20] W. Schreiner, Amawalk, ICDD Grant-in-Aid, Intelligent Controls, Inc. New York, USA, 1991.